Acoustic black hole in Schwarzschild spacetime: Quasinormal modes, analogous Hawking radiation, and shadows

Hong Guo,[1,3,†] Hang Liu,[1,3,‡] Xiao-Mei Kuang,[2,*] and Bin Wang[1,2,§]

[1]*School of Aeronautics and Astronautics, Shanghai Jiao Tong University, Shanghai 200240, China*
[2]*Center for Gravitation and Cosmology, College of Physical Science and Technology, Yangzhou University, Yangzhou 225009, China*
[3]*School of Physics and Astronomy, Shanghai Jiao Tong University, Shanghai 200240, China*

(Received 13 July 2020; revised 13 November 2020; accepted 17 November 2020; published 7 December 2020)

Various properties of acoustic black holes constructed in Minkowski spacetime have been widely studied in the past decades. Recently the acoustic black holes in general spacetime were proposed. In this paper, we first investigate the basic characteristics of "curved" acoustic black holes in Schwarzschild spacetime, including the quasinormal modes, grey-body factor, and analogous Hawking radiation. We find that the signal of the quasinormal mode is weaker than that of the Schwarzschild black hole. Moreover, as the tuning parameter increases, both the positive real part and negative imaginal part of the quasinormal frequency approach to the horizonal axis, but they will not change sign. This means that all the perturbations could die off and the system is stable under those perturbations. Since the larger tuning parameter suppresses the effective potential barrier, so it enhances the grey-body factor. The energy emission rate of Hawking radiation does not monotonically increase the tuning parameter because of the nonmonotonicity of the Hawking temperature. Finally, as a first attempt, we study the acoustic black hole shadow. The radius of the acoustic shadow becomes larger as the tuning parameter increases because both the related acoustic horizon and the acoustic sphere become larger. Our studies could help us to further understand the near horizon geometrical features of the black hole. We also expect that our observations could be detected experimentally in the near future.

DOI: 10.1103/PhysRevD.102.124019

I. INTRODUCTION

The black hole is one of the most intriguing celestial objects in our Universe. It plays a significant role in the study of general relativity (GR), thermodynamics, statistics, and quantum mechanics. Via the astrophysical detections, it is still difficult to touch the signal of Hawking radiation or anything else with the interaction of the quantum field in the gravitational spacetime. The situation turns around when Unruh proposed the acoustic black hole [1], which provides potential connections between astrophysical phenomena and the tabletop experiments.

In the acoustic model of gravity, the equation of motion describes the propagation of sound modes. The acoustic black hole is formed by a moving fluid with speed exceeding the local sound velocity through a spherical surface. The acoustic horizon is the boundary where the speed of flow equals the local speed of sound. The features including horizon, ergosphere, and Hawking radiation of the analogue black holes were explored in [2], inspired by which more efforts on the analogue Hawking radiation were made in [3,4]. Moreover, the stability of the static, or rotating acoustic black holes, has been analyzed via computing the quasinormal modes [5–8]. Readers can refer to [9] for a nice review paper about the analogue black holes.

Experimentally, the first realization of a sonic black hole as Bose–Einstein condensate has been reported in [10]. More recently, the remarkable experiments [11,12] reported that the thermal Hawking radiation and the corresponding temperature in an analogue black hole were observed. Besides, progress on stimulated Hawking radiation has also been made in an optical system [13–15] and some other mechanics [16–18].

Thanks to those significant realizations of astrophysical phenomena in the laboratory, acoustic black holes nowadays attract more and more attention. A more recent extension on the analogue Hawking radiation can be seen in [19–22]. The thermodynamiclike description of the two-dimensional acoustic black hole has been discussed in [23]. The particle dynamics in the acoustic spacetime was also addressed in [24].

Most of the aforementioned studies were based on the acoustic models constructed in the real Minkowski

*Corresponding author.
xmeikuang@yzu.edu.cn
†gh710105@gmail.com
‡hangliu@sjtu.edu.cn
§wang_b@sjtu.edu.cn

spacetime. Nevertheless, the authors of [25–30] derived the acoustic black holes from the relativistic fluids with the starting of the Abelian Higgs model. Especially, by fixing curved spacetime geometry, the authors of [30] studied analogue gravity models by considering the relativistic Gross–Pitaevskii (GP) theory and Yang–Mills theory. They constructed the acoustic black hole in general curved spacetime. This is significant and interesting because the black holes in our Universe could be in the bath of some kind of superfluid or just the cosmological microwave. Moreover, it was addressed in [31] that the acoustic black hole could also emerge from black-D3 brane based on holographic approach.

In this paper, we are interested in the acoustic black hole in four dimensional Schwarzschild background, which could be one of the simplest analogue black holes in curved spacetime. We accept that the characteristics appearing in astrophysical black holes should also appear in their analogous models. Here we shall concentrate on the basic characteristics near the acoustic horizon, which are related to the possible observable quantities of the curved acoustic black hole.

The first characteristic we shall explore is the frequency of quasinormal modes (QNM), which governs the relaxation of the sound wave perturbation. The real part of the QNM frequencies describes the oscillations of the perturbation, while the imaginary part indicates the (un)damped of the mode (see [32] and therein for review). The QNMs of astrophysical black holes have been widely studied because it is one of the fingerprints of a gravity theory or other possible deviations beyond GR. Thus, the study of QNMs could help to test the (in)stability and further provide the stable regime of parameters in acoustic black holes.

The second characteristic we shall investigate is the grey-body factors, which is equal to the transmission probability of an outgoing wave radiated from the black hole event horizon to the asymptotic region [33,34]. The frequency dependent grey-body factors measures the modification of the pure black body spectrum. It gives us significant information about the near-horizon structure of black holes [35]. Moreover, based on the grey-body factors, we shall further evaluate the energy emission rate of analogous Hawking radiation.

The last characteristic we consider is the acoustic black hole shadow. The black hole shadow is another fingerprint of the geometry around the black hole horizon. It describes the black hole properties which depend on the gravitational lensing of the nearby radiation [36]. The black hole shadow is important to determine the near horizon geometry and its properties are widely studied, see for example [37–50] and therein. Moreover, in the experimental side, the Event Horizon Telescope group detected the black hole images with the use of the shadow properties [51–53]. Moveover, the detection of gravitational waves [54] from black holes (or other compact objects) and other observations strongly motivate us to disclose more near horizon geometry of black holes. Thus, as a first attempt we will study the acoustic shadow of the curved acoustic black hole. Theoretically, the acoustic shadow is a region of the listener's sky that is left dumb, if there are sonic sources distributed everywhere but not between the listener and the acoustic black hole. We expect that this observation could be detected in the analogue black hole experiment.

The structure of this paper is listed as follows. In Sec. II, we review the acoustic black hole in the Schwarzschild spacetime and then present the covariant scalar field equation in this background. In Sec. III, we compute the frequencies of quasinormal modes and analyze the stability of the sector under scalar field perturbation. Then in Sec. IV and Sec. V, we study the grey-body factor, Hawking radiation, and the shadow properties of the acoustic black hole, respectively. The last section is our Conclusion and Discussion.

II. BACKGROUND AND THE COVARIANT SCALAR EQUATION

A. Acoustic black hole in Schwarzschild spacetime

In this subsection, we shall first briefly review how the curved acoustic black hole emerges from the GP theory [55], and then we focus on the Schwarzschild acoustic black hole. For more details, readers can refer to [30] where the acoustic black hole in the general curved spacetime has been constructed. The action in GP theory is

$$S = \int d^4x\sqrt{-g}\left(|\partial_\mu\varphi|^2 + m^2|\varphi|^2 - \frac{b}{2}|\varphi|^4\right), \quad (1)$$

where φ is a complex scalar field as order parameter; b is a constant, and m^2 is a temperature dependent parameter assumed as $m^2 \sim (T - T_c)$ [55]. The equation of motion for φ is reduced as

$$\Box\varphi + m^2\varphi - b|\varphi|^2\varphi = 0. \quad (2)$$

One could fix a static background spacetime

$$ds^2_{\rm bg} = g_{tt}dt^2 + g_{rr}dr^2 + g_{\vartheta\vartheta}d\vartheta^2 + g_{\phi\phi}d\phi^2 \quad (3)$$

and set the scalar field as $\varphi = \sqrt{\rho(\vec{x},t)}e^{i\theta(\vec{x},t)}$. In the fixed spacetime, one could assume the background solution of the scalar field as (ρ_0, θ_0), then consider the fluctuations around (ρ_0, θ_0) as

$$\rho = \rho_0 + \rho_1 \quad \text{and} \quad \theta = \theta_0 + \theta_1. \quad (4)$$

By substituting (3)–(4) into the Klein–Gordon equation (2) and considering the long-wavelength limit, one can extract two equations. One is the leading order for the background scalar field

$$b\rho_0 = m^2 - g_{\mu\nu}\partial_\mu\theta_0\partial_\nu\theta_0 = m^2 - v_\mu v^\mu, \tag{5}$$

where in the second equality we have defined $v_0 = -\partial_t\theta_0$, $v_i = \partial_i\theta_0$ $(i = r, \vartheta, \phi)$. The other is a relativistic equation governing the propagation of the phase fluctuation

$$\frac{1}{\sqrt{-\mathcal{G}}}\partial_\mu(\sqrt{-\mathcal{G}}\mathcal{G}^{\mu\nu}\partial_\nu\theta_1) = 0. \tag{6}$$

From the above fluctuation equation, one can extract and derive the effective metric $\mathcal{G}_{\mu\nu}$ as

$$\mathcal{G}_{\mu\nu} = \frac{c_s}{\sqrt{c_s^2 - v_\mu v^\mu}}\begin{pmatrix} g_{tt}(c_s^2 - v_i v^i) & \vdots & -v_i v_t \\ \cdots\cdots\cdots\cdots & \cdot & \cdots\cdots\cdots\cdots\cdots \\ -v_i v_t & \vdots & g_{ii}(c_s^2 - v_\mu v^\mu)\delta^{ij} + v_i v_j \end{pmatrix} \tag{7}$$

with $c_s^2 \equiv \frac{b\rho_0}{2}$. It is obvious that the metric $\mathcal{G}_{\mu\nu}$ encodes both the information of the background spacetime $ds_{\rm bg}$ and the background four velocity of the fluid v_μ.

Following [30], we consider $v_t \neq 0, v_r \neq 0, v_a = 0 (a = \vartheta, \phi), g_{tt}g_{rr} = -1$ and the coordinate transformation $dt \to dt - \frac{v_t v_r}{g_{tt}(c_s^2 - v_r v^r)}dr$. Then the line element of a static acoustic black hole in the background spacetime metric can be reformed from (7) as

$$ds^2 = c_s\sqrt{c_s^2 - v_\mu v^\mu}\left[\frac{c_s^2 - v_r v^r}{c_s^2 - v_\mu v^\mu}g_{tt}dt^2 + \frac{c_s^2}{c_s^2 - v_r v^r}g_{rr}dr^2 + g_{\vartheta\vartheta}d\vartheta^2 + g_{\phi\phi}d\phi^2\right]. \tag{8}$$

We shall focus on the Schwarzschild background spacetime

$$\begin{aligned} ds_{\rm bg}^2 &= g_{tt}dt^2 + g_{rr}dr^2 + g_{\vartheta\vartheta}d\vartheta^2 + g_{\phi\phi}d\phi^2 \\ &= -f(r)dt^2 + \frac{dr^2}{f(r)} + r^2(d\vartheta^2 + \sin^2\vartheta d\phi^2), \end{aligned} \tag{9}$$

where $f(r) = 1 - \frac{2M}{r}$. Subsequently, one can consider an orbit of a vortex that falls freely along the radial from infinity starting from rest outside a Schwarzschild black hole. Then the radial component v_r is treated as the escape velocity of an observer who maintains a stationary position at Schwarzschild coordinate radius r. It can be set as $v_r \sim \sqrt{2M\xi/r}$ in which $\xi > 0$ is required to guarantee the velocity is real. Note that recalling $c_s^2 = \frac{b\rho_0}{2}$ and rescaling $m^2 \to \frac{m^2}{2c_s^2}$, as well as $v^\mu v_\mu \to \frac{v^\mu v_\mu}{2c_s^2}$, Eq. (5) could give us the relation $v_\mu v^\mu = m^2 - 1$. As addressed in [30], one can work at the critical temperature of GP theory such that m^2 vanishes, and then one has $v_\mu v^\mu = -1$. Note that to fulfill the relation $v_\mu v^\mu = -1$, the time component of the velocity in this case can be worked out as $v_t = \sqrt{f(r) + \frac{2M\xi}{r}f(r)^2}$.

To proceed, we rescale $v^\mu v_\mu \to \frac{v^\mu v_\mu}{2c_s^2}$ in (8). Then by substituting the metric functions of (9), $v_r \sim \sqrt{2M\xi/r}$ and $v_\mu v^\mu = -1$ into it, we can rewrite the line element as

$$ds^2 = \sqrt{3}c_s^2\left[-\mathcal{F}(r)dt^2 + \frac{dr^2}{\mathcal{F}(r)} + r^2(d\vartheta^2 + \sin^2\vartheta d\phi^2)\right], \tag{10}$$

with $\mathcal{F}(r) = \left(1 - \frac{2M}{r}\right)\left[1 - \xi\frac{2M}{r}\left(1 - \frac{2M}{r}\right)\right]$, (11)

which is the acoustic black hole metric in Schwarzschild background. Here $\xi > 0$ is defined as the tuning parameter and its regime for the existence of acoustic black holes will be discussed later. It is noticed that (10) recovers the Schwarzschild black hole (9) as $\xi \to 0$, while as $\xi \to +\infty$ the whole spacetime should be an acoustic black hole because the escape velocity v_r goes to infinity. We shall then set $c_s^2 = 1/\sqrt{3}$ for convenience.

Then to fulfill $\mathcal{F}(r) = 0$, we shall obtain three solutions. One is the optical event horizon $r_{bh} = 2M$ and the others are $r_{ac_\pm} = (\xi \pm \sqrt{\xi^2 - 4\xi})M$ for the acoustic black hole. Recalling $\xi > 0$, it is easy to obtain the condition $\xi \geq 4$ to make sure the existence of acoustic horizons. When $\xi = 4$, the acoustic black hole goes to the extreme case with $r_{ac_-} = r_{ac_+} = 4M$. We plot the dependence of $r_{ac_\pm}$ on ξ in Fig. 1. The inner acoustic horizon is confined in $r_{ac_-} \in (2M, 4M)$ (the red dashed line), which denotes that the acoustic horizon locates outside the real black hole as expected. The outer horizon r_{ac_+} (the red line) grows monotonously as ξ increases. When $\xi \to \infty$, we have $r_{ac_+} \to \infty$ meaning that the sound could not escape from the whole spacetime as we aforementioned. In a word, in the case with $\xi \geq 4$, an analogue metric would involve the Schwarzschild spacetime such that the spacetime can be divided into four regions: the inside of black hole is in the regime $r < r_{bh}$; in the regime $r_{bh} < r < r_{ac_-}$ and $r_{ac_-} < r < r_{ac_+}$, the light can escape but the sound cannot;

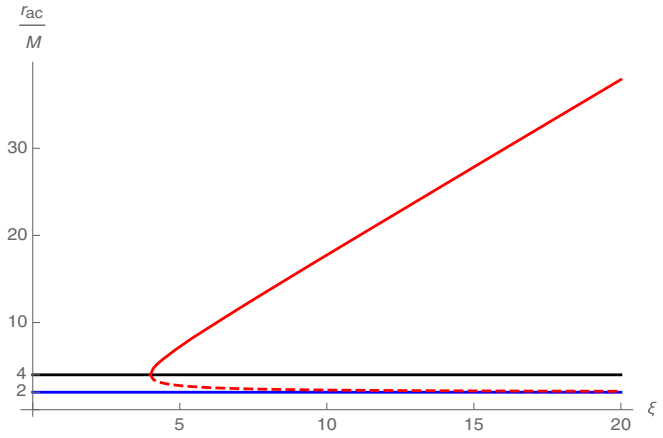

FIG. 1. The relation of the ratio of $r_{ac_\pm}/M$ and the tuning parameter ξ.

while in the regime $r > r_{ac_+}$, both the light and the sound could escape. Note that in the following study, the acoustic horizon represents the outer horizon, i.e., we could set $r_{ac} = r_{r_{ac_+}}$.

B. Covariant scalar equation

We are interested in some basic characteristics of this acoustic black hole, including quasinormal modes and grey-body factors of scalar fields as well as the shadow cast. To this end, we consider the minimally coupled massless scalar field as a probe. Its covariant equation is

$$\frac{1}{\sqrt{-\mathcal{G}}}\partial_\mu(\sqrt{-\mathcal{G}}\mathcal{G}^{\mu\nu}\partial_\nu\psi) = 0, \tag{12}$$

where $\mathcal{G}_{\mu\nu}$ denotes the metric components of the acoustic black holes (10). Taking the standard ansatz

$$\psi(t, r, \theta) = \sum_{lm} e^{-i\omega t}\frac{\Psi(r)}{r}Y_{lm}(\theta) \tag{13}$$

and introducing the tortoise coordinate $r_* = \int 1/\mathcal{F}dr$, we shall obtain the Schrodinger-like formula

$$\frac{d^2\Psi}{dr_*^2} + (\omega^2 - V(r))\Psi = 0, \tag{14}$$

where the effective potential is

$$V(r) = \mathcal{F}\left[\frac{l(l+1)}{r^2} + \frac{\mathcal{F}'}{r}\right]. \tag{15}$$

The radial domain of the following study is given by $r \in (r_{ac}, \infty)$.

The effective potential as a function of r for different cases are present in Fig. 2. As the radial coordinate approaches to the near horizon region, the effective potential first shows a barrier and then quickly falls into zero at the acoustic horizon, meanwhile, the tortoise coordinate r_* reaches the infinity $r_* \to -\infty$. In the left plot, with fixed ξ and M, the position of zero potential is not affected by the angular number, which is reasonable because it has no print on the acoustic horizon. However, the potential barrier is promoted by larger l, which is similar to that in Schwarzschild black hole. On the right plot, as we increase the tuning parameter, the position of zero potential is located at larger radius because the acoustic horizon increases (see Fig. 1). In addition, the potential barrier is suppressed by larger ξ. This behavior could be reflected by the near horizon characteristics as we will show soon.

III. QUASINORMAL MODES

In this section we shall study the quasinormal modes from the Eq. (14). Thus, we require the purely outgoing waves at infinity and purely incoming waves at the acoustic horizon for the scalar field as

$$\Psi \sim e^{\pm i\omega r_*}, \qquad r_* \to \pm\infty. \tag{16}$$

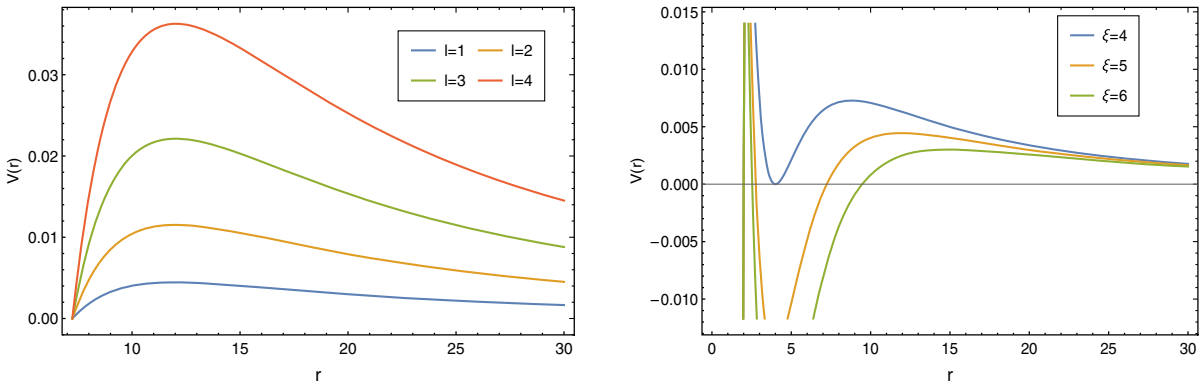

FIG. 2. The behavior of effective potential with $M = 1$. On the left panel we fix $\xi = 5$ and take different angular numbers into consideration, while on the right panel we show the potential at fixed $l = 1$ for different ξ.

TABLE I. The QNM frequency of acoustic black holes with the mode $l = n = 0$.

ξ	Ninth-order WKB	AIM
0	$0.11031 - 0.10496i$	–
4	$0.02836 - 0.01905i$	–
5	$0.02341 - 0.01656i$	$0.02351 - 0.01660i$
6	$0.01954 - 0.01471i$	$0.01956 - 0.01471i$
7	$0.01668 - 0.01310i$	$0.01666 - 0.01307i$
8	$0.01469 - 0.01168i$	$0.01449 - 0.01171i$
9	$0.01283 - 0.01066i$	$0.01282 - 0.01058i$
10	$0.01148 - 0.00971i$	$0.01149 - 0.00964i$

To calculate the frequency of the QNMs, we employ the semianalytical WKB method and the asymptotic iteration method (AIM), both of which are widely applied in the study of QNMs. Here we skip the instruction of the two methods, and the readers can refer to [56,57] (and therein) for the details, respectively. It is noticed that even though our results are quite at good convergence in the sixth-order WKB approximation, our calculation is accomplished by the WKB method up to the ninth-order correction for sufficient precision.

The QNM frequencies for small ξ with samples of angular number l and overtone number n are listed in Table I ($l = n = 0$), Table II ($l = 1$, $n = 0$), and Table III ($l = n = 1$), respectively. The universal properties of the QNM frequency we can extract from the three tables are:

(i) The real part $\mathrm{Re}(\omega)$ is positive and the imaginal part $\mathrm{Im}(\omega)$ is negative, which means the acoustic black holes are stable under the perturbation for small tuning parameters. Moreover, their magnitudes for the acoustic black hole are quite smaller than that for the Schwarzschild black hole with $\xi = 0$. This implies that the signal of the QNM is weaker in acoustic black holes than in the astrophysical black hole, so the perturbation dies off slower.

(ii) With the increasing of ξ, the real part of the frequency decreases. It means that the oscillation of the scalar field damps. The magnitude of the imaginal part also decreases, denoting the loss of the damping rate. These results imply that the strength of oscillation is damping as the acoustic horizon r_{ac} grows because r_{ac} is larger as ξ increases (see Fig. 1). This behavior is reasonable because the effective potential barrier is suppressed by larger acoustic black holes (see Fig. 2).

(iii) In each table, the magnitude of $\mathrm{Im}(\omega)$ continues decreasing as ξ increases. This indicates that the $\mathrm{Im}(\omega)$ may cross zero and changes sign as we continue increasing ξ. Since the system is stable only when $\mathrm{Im}(\omega)$ is always negative, therefore, to further check the stability, we must study the QNM frequency for general ξ.

TABLE II. The QNM frequency of acoustic black holes with the mode $l = 1$ and $n = 0$.

ξ	Ninth-order WKB	AIM
0	$0.29294 - 0.09766i$	–
4	$0.08211 - 0.01744i$	–
5	$0.06391 - 0.01591i$	$0.06390 - 0.01591i$
6	$0.05234 - 0.01402i$	$0.05234 - 0.01402i$
7	$0.04434 - 0.01240i$	$0.04434 - 0.01240i$
8	$0.03848 - 0.01107i$	$0.03848 - 0.01107i$
9	$0.03399 - 0.00998i$	$0.03399 - 0.00998i$
10	$0.03045 - 0.00908i$	$0.03045 - 0.00908i$

TABLE III. The QNM frequency of acoustic black holes with the mode $l = n = 1$.

ξ	Ninth-order WKB	AIM
0	$0.26431 - 0.30620i$	–
4	$0.07649 - 0.05359i$	–
5	$0.06061 - 0.04869i$	$0.06061 - 0.04868i$
6	$0.04947 - 0.04314i$	$0.04947 - 0.04313i$
7	$0.04171 - 0.03829i$	$0.04171 - 0.03828i$
8	$0.03603 - 0.03426i$	$0.03604 - 0.03426i$
9	$0.03171 - 0.03095i$	$0.03171 - 0.03095i$
10	$0.02832 - 0.02818i$	$0.02832 - 0.02818i$

The QNM frequencies as a function of general tuning parameter are shown in Fig. 3 and Fig. 4 where we choose samples of modes with fixed $l = 1$ and $n = 0$, respectively. The features of the QNM frequency we can obtain from the figures are summarized as follows:

(i) In both figures, as ξ increases, both the positive real part and negative imaginary part are close to the horizontal axis, but neither of them changes sign. This indicates that all the perturbation could die off and the acoustic black hole is stable under those perturbations. It is noticed that similar behavior was observed for the counter-rotating waves (negative l) as the rotation parameter increases in the rotating acoustic flat black hole [5].

(ii) In Fig. 3 with fixed $l = 1$, different overtones have different QNM frequencies and the difference is more sharp at small ξ. Moreover, for larger n, both $\mathrm{Re}(\omega)$ and $\mathrm{Im}(\omega)$ are suppressed, which implies that perturbation with larger n die off quicker. This property is similar as that for acoustic black holes in flat spacetime as well as that for Schwarzschild black holes.

(iii) In Fig. 4 with fixed overtone, different modes correspond to different QNM frequencies. As l increases, both $\mathrm{Re}(\omega)$ and $\mathrm{Im}(\omega)$ are enhanced, indicating that the perturbation with smaller l dies off quicker. This property also matches that in acoustic black holes in flat spacetime and Schwarzschild black holes.

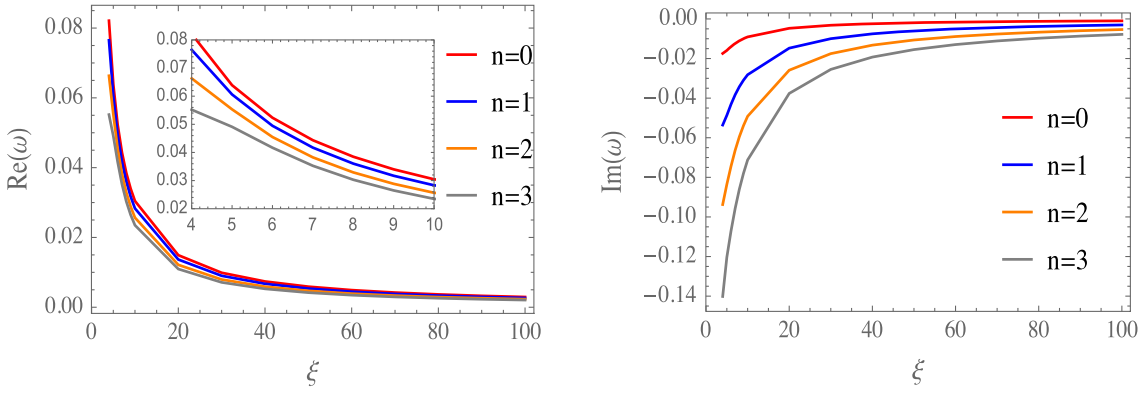

FIG. 3. The QNM frequency as a function of ξ for different overtone numbers with fixed $l = 1$.

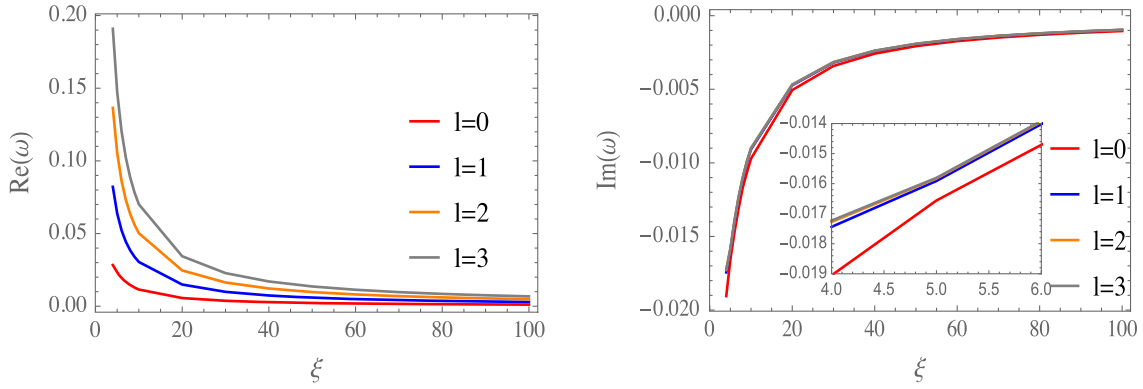

FIG. 4. The QNM frequency as a function of ξ for different angular numbers with fixed $n = 0$.

Then we further study the effect of mass M on the QNM frequency. The results with fixed $\xi = 5$ and $l = n = 0$ are shown in Fig. 5. It is obvious that as M increases, the positive $\mathrm{Re}(\omega)$ decreases and approaches to zero, while the negative $\mathrm{Im}(\omega)$ increases and also approaches to the horizonal axis. We did not find the sign changing as we further increase M, such that the sector is stable. This behavior indicates that the existence of heavier black holes or other compact objects would restrain the oscillation amplitude of the scalar field, even though it could die off slower. It is noticed that the rule is similar as to the effect of ξ because both larger M and ξ corresponds to larger acoustic black holes.

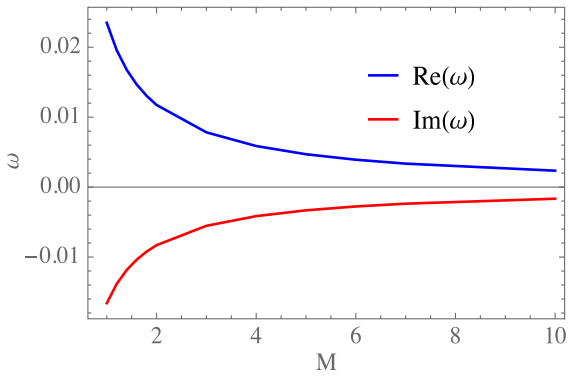

FIG. 5. The quasinormal modes as a function of M with fixed $\xi = 5$ and $l = n = 0$.

IV. GREY-BODY FACTOR AND HAWKING RADIATION

In this section we investigate the grey-body factor and analogue Hawking radiation of the acoustic black hole. The existence of an acoustic horizon implies the emission of a thermal flux of phonons, named analogue Hawking radiation, and the temperature is proportional to the gradient of the velocity field at the acoustic horizon.

There are plenty of approaches proposed to study the Hawking radiation for astrophysical black holes. It is known that the radiation is not exactly of a black-body type since the particles which are created in the vicinity of the event horizon without enough energy cannot penetrate the potential barrier. So only part of the particles can be observed at infinity, which makes it just a scattering problem. Thus, to get the transmission probability of particles, we solve the wave equation outside the black hole (acoustic black hole in our present consideration) and calculate the scattering coefficient by which the grey-body

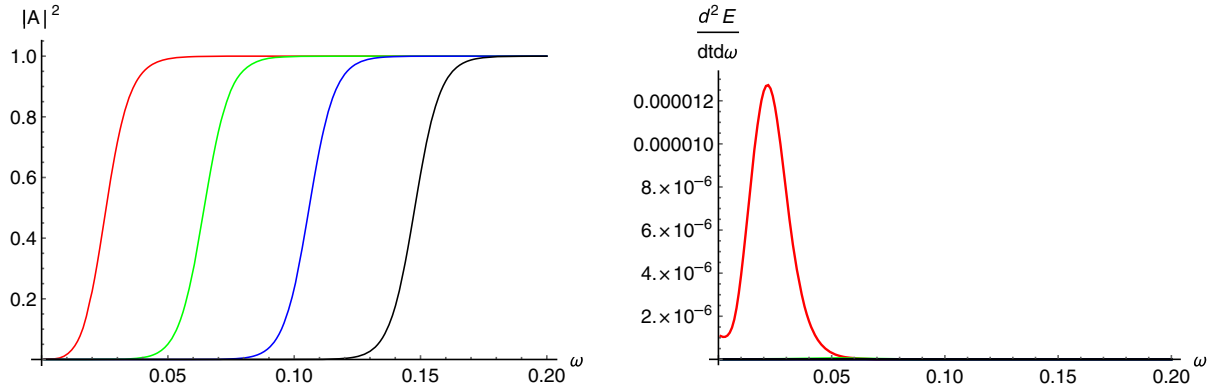

FIG. 6. The left panel shows the grey-body factor and the right panel shows the partial energy radiation rate for different angular numbers. For both panels, we fix $\xi = 5$, and the red, green, blue, and black lines correspond to angular numbers $l = 0$, 1, 2, and 3, respectively. On the right plot, the radiation rate for $l > 0$ are too weak to be observable.

factor can be obtained. We use the grey-body factor to describe the transmission of particles through the potential, and thus work out the energy radiation rate based on the obtained grey-body factor. Note that the effective potential presents a barrier which monotonically decreases as the radius coordinate r_* approaches both infinities. This behavior allows us to use the WKB approach to compute the grey-body factor.

We should consider the wave equation, Eq. (14), with the boundary condition allowing the incoming waves from infinity. This is different from that for computing QNMs, where only outgoing waves are allowed in the infinity. The scattering boundary condition is given by

$$\Psi = Te^{-i\omega r_*}, \qquad r_* \to -\infty, \tag{17}$$

$$\Psi = e^{-i\omega r_*} + \mathrm{Re}^{i\omega r_*}, \qquad r_* \to +\infty, \tag{18}$$

where R and T are the reflection and transmission coefficients satisfying $|T|^2 + |R|^2 = 1$. The grey-body factor is then given by the transmission coefficient for each angular number as [58]

$$|A_l|^2 = 1 - |R_l|^2 = |T_l|^2 \quad \text{and} \quad |T_l|^2 = (1 + e^{2i\pi K})^{-1}, \tag{19}$$

where K is determined by the equation

$$K = i\frac{\omega^2 - V_0}{\sqrt{-2V_0''}} - \sum_{i=2}^{i=6} \Lambda_i(K). \tag{20}$$

Here V_0 and V_0'' denotes the maximal value of the effective potential and its second derivative with respective to the tortoise coordinate at the maximum, respectively; and Λ_i are the higher WKB corrections which are dependent on K and up to $2i$th-order derivative of the potential at its maximum [58–60]. We briefly review how to derive $\Lambda_i(K)$ in Appendix.

Once the grey-body factor is at hand, we can then study the Hawking radiation by evaluating the energy emission rate which is connected with the grey-body factor via [61]

$$\frac{dE}{dt} = \sum_l N_l |A_l|^2 \frac{\omega}{e^{\omega/T_H} - 1}\frac{d\omega}{2\pi}. \tag{21}$$

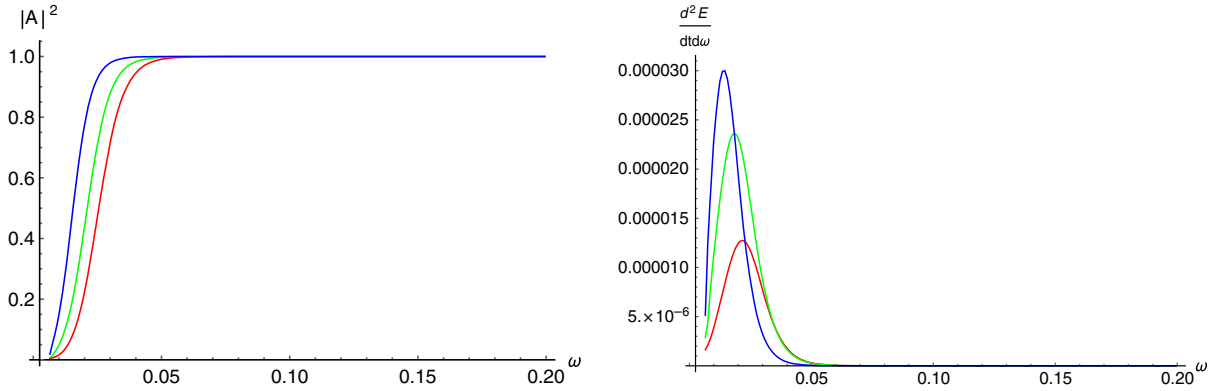

FIG. 7. The left panel shows the grey-body factor and the right panel shows the partial energy radiation rate for different ξ. For both panels, we fix $l = 0$, and the red line, green line, and blue line correspond to $\xi = 5$, $\xi = 6$, and $\xi = 8$, respectively.

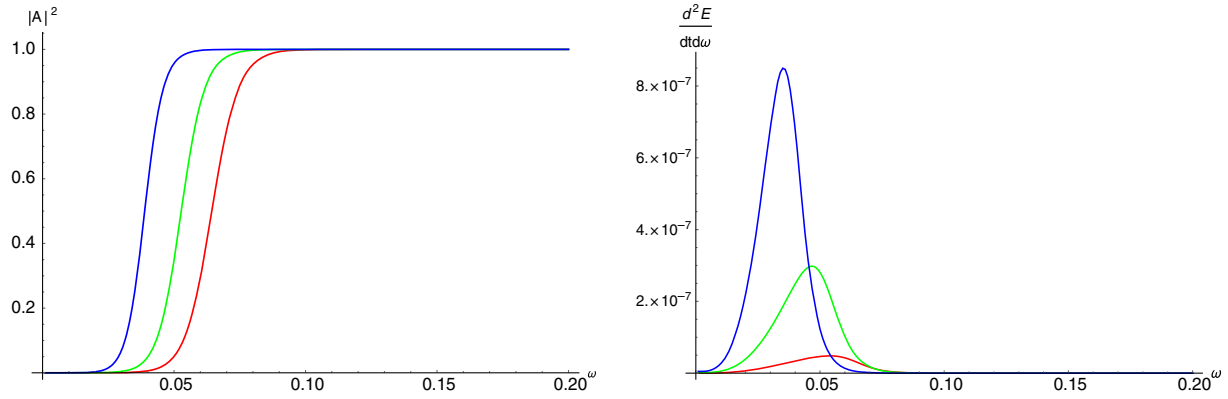

FIG. 8. The left panel shows the grey-body factor and the right panel shows the partial energy radiation rate for different ξ. For both panels, we fix $l = 1$, and the red line, green line, and blue line correspond to $\xi = 5$, $\xi = 6$, and $\xi = 8$, respectively.

In the above definition, T_H is the analogue Hawking temperature defined as $T_H = -\mathcal{F}'(r_{ac})/4\pi$, and N_l are the multiplicities satisfying $N_l = 2l + 1$ for the scalar field.

Then, we shall employ the sixth-order WKB method to calculate the grey-body factor and energy emission rate of Hawking radiation. It is noticed that this method was employed to study the properties of Hawking radiation in various models, see for examples [62–65] and therein. Our results are shown in Figs. 6–8.

In Fig. 6 we fix the tuning parameter $\xi = 5$ and study the effect of the angular number l. The left panel shows that the larger frequency corresponds to the higher grey-body as a natural consequence of the fact that the particles with larger energy are more likely to penetrate the potential barrier. On the other hand, it is obvious that a larger angular number leads to a lower grey-body factor. This result can be intuitively explained by the effective potential which has a higher barrier for larger l (see Fig. 2), such that the particles are more likely to be reflected by the potential. The energy emission rate of the Hawking radiation is shown in the right panel. It is observed that the mode with $l = 0$ dominates the Hawking radiation, while the contribution of modes with higher l is very small and negligible.

In Fig. 7 and Fig. 8, we choose different tuning parameters and fix the angular number $l = 0$ and $l = 1$, respectively. The behaviors in the two figures are qualitatively similar with an obvious exception that the energy radiation rate for $l = 0$ is much stronger than that for $l = 1$. The left panels in the figures show that the grey-body factor is enhanced by larger ξ because of the lower potential barrier as we have shown in Fig. 2. In the right panels, the emission rate at the low frequency region for larger ξ is larger, but when ω grows larger, this picture will be changed as a result of its Hawking temperature dependence. It is shown in Fig. 9 that the Hawking temperature grows from zero, which corresponds the extremal black holes at $\xi = 4$ to a maximum at $\xi = 16/3$, and then it decreases to suppress the energy emission rate.

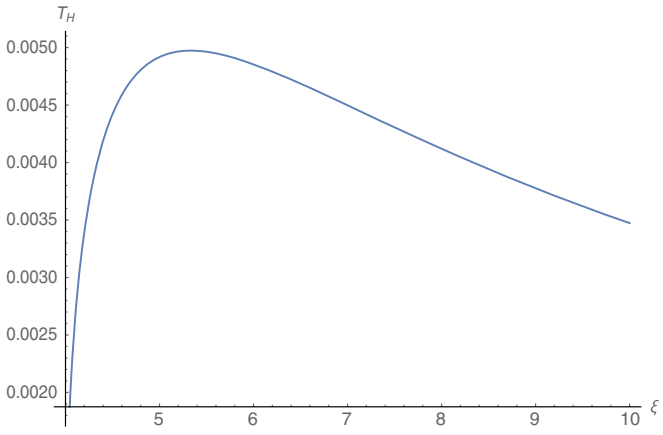

FIG. 9. The behavior of Hawking temperature as a function of ξ. Here we take $M = 1$.

V. ACOUSTIC BLACK HOLE SHADOW

The black hole shadow in GR is one of the optical properties. As a first attempt, we shall study the analogous behavior in the acoustic black hole. We treat it as "acoustic shadow" which describes the property of the sound waves. Analogous with the gravitational lensing and the related properties of astrophysical black holes, there exists the inmost unstable sound wave orbit, and we call it "acoustic sphere" instead of "photon sphere." Beyond the acoustic sphere, the sound waves are absorbed by the acoustic black hole, so the acoustic sphere describes the "audible" boundary of the sound waves near the acoustic black hole horizon region. This property is related to the acoustic shadow.

Moreover, it is known that the shadow for static and spherical symmetric black holes also has spherical symmetry. The shape of shadow would be more complex when the rotation of the black hole is involved. Thus, here for the static and spherical symmetric acoustic black hole (10), we simply study the shadow radius and discuss how the tuning

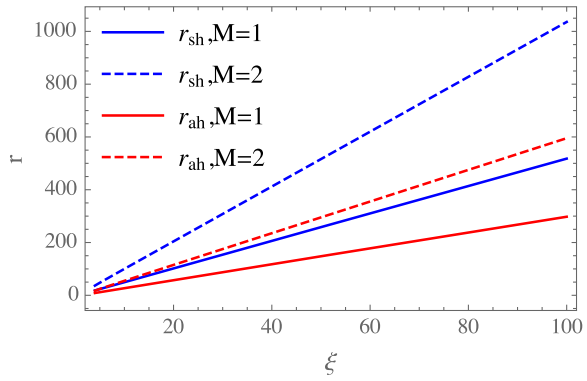

FIG. 10. The shadow radius r_{sh} and the acoustic sphere r_{ah} changing with the tuning parameter ξ.

parameter and the black hole mass shall affect the shadow radius.

To proceed, we follow the designations of [66] and find the radius of the acoustic sphere r_{ah} by solving the following equation:

$$\frac{dh^2(r)}{dr} = 0, \tag{22}$$

where the function $h(r)$ is defined as $h(r) = \sqrt{r^2/\mathcal{F}(r)}$. Then for a distant static listener locating at r_L, the detected radius of the acoustic shadow is

$$r_{sh} = \frac{h(r_{ah})r_L}{h(r_L)}. \tag{23}$$

To study the properties of the acoustic shadow, we assume the static listener is far away from the vicinity of the acoustic horizon so that we have $\frac{r_L}{h(r_L)} \approx 1$. The radius of the acoustic sphere and the acoustic shadow as functions of the tuning parameter are given in Fig. 10. It is obvious that with fixed M, both r_{sh} and r_{ah} increase almost linearly as ξ, but the slope for the shadow radius is larger than that for the acoustic sphere. Moreover, in the figure, we can also see the influence of the mass parameter M on the radius, that the larger M corresponds to both larger shadow radius and acoustic radius. This is reasonable because the increase of M could enlarge the acoustic horizon. It is noticed that the radius of the acoustic sphere is much larger than the photon sphere for the Schwarzschild black hole, which is $3M$.

VI. CONCLUSION AND DISCUSSION

In this paper, we explored the near-horizon characteristic of the curved acoustic black hole in the Schwarzschild spacetime. By considering the minimal coupling massless scalar field, we studied the quasinormal mode, grey-body factor, and analogous Hawking radiation of the sector. Moreover, as a first attempt, we also studied the acoustic shadow which is analogous to the photon shadow caused by the bent light ray in general relativity.

We computed the frequencies of QNMs with the use of the WKB method up to ninth-order corrections as well as the asymptotic iteration method. Our results showed that the signal of QNMs in this acoustic black hole is weaker than that in a Schwarzschild black hole. Moreover, the real part is always positive while the imaginal part of the QNM frequency is negative, and both of them get closer to the horizonal axis as the tuning parameter increases. The sign of the QNM frequency does not change, which implies that all the perturbations would die off and the acoustic black hole is stable under those perturbations. It would be interesting to further test the stability under other types of perturbations around the acoustic black hole, which will be present elsewhere.

We then investigated the analogous Hawking radiation of the acoustic black hole. We employed the WKB approach to solve the scalar equation as a scattering problem. Both the grey-body factor and the energy emission rate of Hawking radiation are affected by the angular number and the tuning parameter which correspond to different properties of the potential barrier. Especially, the grey-body factor is enhanced by the larger tuning parameter because it corresponds to a lower potential barrier. The energy emission rate of Hawking radiation is not a monotonic function of the tuning parameter due to the nonmonotonicity of the Hawking temperature.

Finally, we studied the acoustic shadow of acoustic black holes. Since the acoustic black hole we considered is static and spherically symmetric, so the acoustic shadow also has spherical symmetry. Thus, we simply analyzed the acoustic shadow radius, and we found that the radius of the shadow becomes larger as the tuning parameter increases. This is acceptable because as the parameter increases, both the acoustic horizon and the acoustic sphere increases.

It is worthwhile to mention that our work is the first attempt to study the "black hole shadow" in the acoustic black hole. Though here we worked with the techniques developed in the optical case, one could expect experimental interest in the acoustic shadow due to the following two aspects. On one hand, as we mentioned in the introduction, the experimental simulation of the analogous black hole is significant for us to understand astrophysical phenomena. The acoustic shadow is a direct observable quantity which would shed light on the experimental simulation of the acoustic black hole. Especially, the acoustic shadow is a great indicator to describe the near acoustic horizon region in the laboratory, so the study of acoustic shadow could help us further "touch" the essences of the real black hole. On the other hand, the study on this topic could be a good chance to detect the motion of the sound waves in a medium. The experimental study of the

acoustic shadow could be a possible clue to understand the similarity and differences between the sonic fluid and the black hole geometry. Indeed, there have been some attempts in this direction, for instance, the sound wave shadow zone in a stratified ocean was studied in [67] many yeas ago. Inspired by this work, people found the zero-reflection effects of the sound waves [68–70] in which the authors associated the properties with the "black holes" effect.

It is expected that most of the black holes in the galactic center rotate. Moreover, rotating black holes are closely related with the two important directions: the gravitational waves and black hole shadows, which open new windows for us to understand the Universe. Thus, it would be significant to extend our studies into the acoustic black hole with rotation in the curved spacetime, and then further study the connection between QNM frequency and shadow, which was proposed in [71]. We also expect that our theoretical results could be observed in analogous black hole experiments in the near future. This could help us to further understand the structure of near horizon geometry of astrophysical black holes.

ACKNOWLEDGMENTS

This work is supported by the Natural Science Foundation of China under Grants No. 11705161 and No. 11835009, Fok Ying Tung Education Foundation under Grant No. 171006, and the Natural Science Foundation of Jiangsu Province under Grant No. BK20170481.

APPENDIX: HIGHER ORDER CORRECTION TERMS $\Lambda_i(K)$ OF WKB APPROACH

In this Appendix, we shall follow [58] and briefly introduce how to fix the higher order correction terms $\Lambda_i(K)$ as we show in Eq. (20) for the WKB method. Note that Λ_2 and Λ_3 are derived in the following and one can refer to Ref. [60] for the more higher terms Λ_4, Λ_5, and Λ_6.

We first write the master equation in the form

$$\epsilon^2 \frac{d^2\psi}{dx^2} + Q(x)\psi(x) = 0, \tag{A1}$$

where ϵ is the perturbation parameter introduced to keep track of orders in the WKB approximations. We carry out Taylor expansion to $Q(x)$ about the point x_0 at which $-Q(x)$ reaches maximum. We have the expansion

$$Q(x) = Q_0 + \frac{1}{2}Q_0''z^2 + \frac{1}{6}Q_0'''z^3 + \frac{1}{24}Q_0^{(4)}z^4 + \frac{1}{120}Q_0^{(5)}z^5 + \frac{1}{720}Q_0^{(6)}z^6, \tag{A2}$$

where $z = x - x_0$. Then the master equation (A1) can be rewritten as

$$\epsilon^2 d^2\psi/dz^2 + k(-z_0^2 + z^2 + bz^3 + cz^4 + dz^5 + fz^6)\psi = 0, \tag{A3}$$

where

$$k = \frac{1}{2}Q_0'', \qquad z_0^2 = -2\frac{Q_0}{Q_0''}, \qquad b = \frac{1}{3}\frac{Q_0'''}{Q_0''} \tag{A4}$$

$$c = \frac{1}{12}\frac{Q_0^{(4)}}{Q_0''}, \qquad d = \frac{1}{60}\frac{Q_0^{(5)}}{Q_0''}, \qquad f = \frac{1}{360}\frac{Q_0^{(6)}}{Q_0''}. \tag{A5}$$

Introducing a new variable $t \propto z/\epsilon^{1/2}$, we could define constants $\nu, \Lambda_2, \Lambda_3$ and then rescale the parameters b, c, d, f as

$$t = (4k)^{1/4}e^{-i\pi/4}z/\epsilon^{1/2} \tag{A6}$$

$$K \equiv \nu + \frac{1}{2} = -ik^{1/2}z_0^2/2\epsilon - \epsilon\Lambda_2 - \epsilon^2\Lambda_3 \tag{A7}$$

$$\bar{b} = \frac{1}{4}b(4k)^{-1/4}e^{i\pi/4}, \qquad \bar{c} = \frac{1}{4}c(4k)^{-1/2}e^{i\pi/2} \tag{A8}$$

$$\bar{d} = \frac{1}{4}d(4k)^{-3/4}e^{3i\pi/4}, \qquad \bar{f} = \frac{1}{4}f(4k)^{-1}e^{i\pi}. \tag{A9}$$

Then, Eq. (A3) takes the form

$$\frac{d^2\psi}{dt^2} + \left(K - \frac{1}{4}t^2 - \epsilon^{1/2}\bar{b}t^3 + \epsilon(\Lambda_2 - \bar{c}t^4) - \epsilon^{3/2}\bar{d}t^5 + \epsilon^2(\Lambda_3 - \bar{f}t^6)\right)\psi = 0. \tag{A10}$$

One can refer to [58] for the further process following (A10). Here we shall turn our attention to the expressions of correction terms Λ_2, Λ_3

$$\Lambda_2 = \frac{1}{2}(3\bar{c} - 7\bar{b}^2) + K^2(6\bar{c} - 30\bar{b}^2) \tag{A11}$$

$$\Lambda_3 = -K(1155\bar{b}^4 - 918\bar{b}^2\bar{c} + 67\bar{c}^2 + 190\bar{b}\bar{d} - 25\bar{f}) - K^3(2820\bar{b}^4 - 1800\bar{b}^2\bar{c} + 68\bar{c}^2 + 280\bar{b}\bar{d} - 20\bar{f}). \tag{A12}$$

Note that according to Eq. (A7), we take $\epsilon = 1$, $Q(x) = \omega^2 - V(x)$, $Q(x_0) = Q_0 = \omega^2 - V_0$ then we reduces to the third-order WKB formula of Eq. (20) as

$$K = i\frac{\omega^2 - V_0}{\sqrt{-2V_0''}} - \Lambda_2(K) - \Lambda_3(K). \tag{A13}$$

[1] W. G. Unruh, Experimental Black-Hole Evaporation?, Phys. Rev. Lett. **46**, 1351 (1981).

[2] M. Visser, Acoustic black holes: Horizons, ergospheres, and Hawking radiation, Classical Quantum Gravity **15**, 1767 (1998).

[3] L.-C. Zhang, H.-F. Li, and R. Zhao, Hawking radiation from a rotating acoustic black hole, Phys. Lett. B **698**, 438 (2011).

[4] H. Vieira and V. Bezerra, Acoustic black holes: Massless scalar field analytic solutions and analogue Hawking radiation, Gen. Relativ. Gravit. **48**, 88 (2016).

[5] V. Cardoso, J. P. Lemos, and S. Yoshida, Quasinormal modes and stability of the rotating acoustic black hole: Numerical analysis, Phys. Rev. D **70**, 124032 (2004).

[6] H. Nakano, Y. Kurita, K. Ogawa, and C.-M. Yoo, Quasinormal ringing for acoustic black holes at low temperature, Phys. Rev. D **71**, 084006 (2005).

[7] E. Berti, V. Cardoso, and J. P. Lemos, Quasinormal modes and classical wave propagation in analogue black holes, Phys. Rev. D **70**, 124006 (2004).

[8] S.-B. Chen and J.-L. Jing, Quasinormal modes of a coupled scalar field in the acoustic black hole spacetime, Chin. Phys. Lett. **23**, 2210 (2006).

[9] C. Barcelo, S. Liberati, and M. Visser, Analogue gravity, Living Rev. Relativity **8**, 12 (2005).

[10] O. Lahav, A. Itah, A. Blumkin, C. Gordon, and J. Steinhauer, Realization of a Sonic Black Hole Analogue in a Bose-Einstein Condensate, Phys. Rev. Lett. **105**, 240401 (2010).

[11] J. R. M. de Nova, K. Golubkov, V. I. Kolobov, and J. Steinhauer, Observation of thermal Hawking radiation and its temperature in an analogue black hole, Nature (London) **569**, 688 (2019).

[12] M. Isoard and N. Pavloff, Departing from Thermality of Analogue Hawking Radiation in a Bose-Einstein Condensate, Phys. Rev. Lett. **124**, 060401 (2020).

[13] J. Steinhauer, Observation of self-amplifying hawking radiation in an analogue black-hole laser, Nat. Phys. **10**, 864 (2014).

[14] J. Drori, Y. Rosenberg, D. Bermudez, Y. Silberberg, and U. Leonhardt, Observation of Stimulated Hawking Radiation in an Optical Analogue, Phys. Rev. Lett. **122**, 010404 (2019).

[15] Y. Rosenberg, Optical analogues of black-hole horizons, Phil. Trans. R. Soc. A **378**, 20190232 (2020).

[16] Y. Guo and Y.-G. Miao, Quasinormal mode and stability of optical black holes in moving dielectrics, Phys. Rev. D **101**, 024048 (2020).

[17] A. Bera and S. Ghosh, Stimulated Hawking emission from electromagnetic analogue black hole: Theory and observation, Phys. Rev. D **101**, 105012 (2020).

[18] M. P. Blencowe and H. Wang, Analogue gravity on a superconducting chip, Phil. Trans. R. Soc. A **378**, 20190224 (2020).

[19] M. Anacleto, F. Brito, C. Garcia, G. Luna, and E. Passos, Quantum-corrected rotating acoustic black holes in Lorentz-violating background, Phys. Rev. D **100**, 105005 (2019).

[20] R. Balbinot, A. Fabbri, R. A. Dudley, and P. R. Anderson, Particle production in the interiors of acoustic black holes, Phys. Rev. D **100**, 105021 (2019).

[21] G. Eskin, New examples of Hawking radiation from acoustic black holes, arXiv:1906.06038.

[22] G. Eskin, Hawking type radiation from acoustic black holes with time-dependent metric, arXiv:1912.12775.

[23] B. Zhang, Thermodynamics of acoustic black holes in two dimensions, Adv. High Energy Phys. **2016**, 5710625 (2016).

[24] Q. Wang and X.-H. Ge, On the geometry outside of acoustic black holes in $2+1$-dimensional spacetime, Phys. Rev. D **102**, 104009 (2020).

[25] X.-H. Ge and S.-J. Sin, Acoustic black holes for relativistic fluids, J. High Energy Phys. 06 (2010) 087.

[26] X.-H. Ge, S.-F. Wu, Y. Wang, G.-H. Yang, and Y.-G. Shen, Acoustic black holes from supercurrent tunneling, Int. J. Mod. Phys. D **21**, 1250038 (2012).

[27] M. Anacleto, F. Brito, and E. Passos, Acoustic black holes from Abelian Higgs model with Lorentz symmetry breaking, Phys. Lett. B **694**, 149 (2010).

[28] M. Anacleto, F. Brito, and E. Passos, Supersonic velocities in noncommutative acoustic black holes, Phys. Rev. D **85**, 025013 (2012).

[29] X.-H. Ge, J.-R. Sun, Y. Tian, X.-N. Wu, and Y.-L. Zhang, Holographic interpretation of acoustic black holes, Phys. Rev. D **92**, 084052 (2015).

[30] X.-H. Ge, M. Nakahara, S.-J. Sin, Y. Tian, and S.-F. Wu, Acoustic black holes in curved spacetime and the emergence of analogue Minkowski spacetime, Phys. Rev. D **99**, 104047 (2019).

[31] C. Yu and J.-R. Sun, Note on acoustic black holes from black D3-brane, Int. J. Mod. Phys. D **28**, 1950095 (2019).

[32] V. Cardoso, Quasinormal modes and gravitational radiation in black hole spacetimes, arXiv:gr-qc/0404093.

[33] Y. Myung and H. Lee, No absorption in de Sitter space, Classical Quantum Gravity **20**, 3533 (2003).

[34] T. Harmark, J. Natario, and R. Schiappa, Greybody factors for d-dimensional black holes, Adv. Theor. Math. Phys. **14**, 727 (2010).

[35] P. Kanti and J. March-Russell, Calculable corrections to brane black hole decay. 1. The scalar case, Phys. Rev. D **66**, 024023 (2002).

[36] P. V. P. Cunha and C. A. R. Herdeiro, Shadows and strong gravitational lensing: A brief review, Gen. Relativ. Gravit. **50**, 42 (2018).

[37] M. Amir, A. Banerjee, and S. D. Maharaj, Shadow of charged wormholes in Einstein–Maxwell–dilaton theory, Ann. Phys. (Amsterdam) **400**, 198 (2019).

[38] M. Amir, K. Jusufi, A. Banerjee, and S. Hansraj, Shadow images of Kerr-like wormholes, Classical Quantum Gravity **36**, 215007 (2019).

[39] K. Jusufi, M. Jamil, P. Salucci, T. Zhu, and S. Haroon, Black hole surrounded by a dark matter halo in the M87 Galactic Center and its identification with shadow images, Phys. Rev. D **100**, 044012 (2019).

[40] S. Haroon, K. Jusufi, and M. Jamil, Shadow images of a rotating dyonic black hole with a global monopole surrounded by perfect fluid, Universe **6**, 23 (2020).

[41] S. Vagnozzi, C. Bambi, and L. Visinelli, Concerns regarding the use of black hole shadows as standard rulers, Classical Quantum Gravity **37**, 087001 (2020).

[42] A. Allahyari, M. Khodadi, S. Vagnozzi, and D. F. Mota, Magnetically charged black holes from non-linear electrodynamics and the Event Horizon Telescope, J. Cosmol. Astropart. Phys. 02 (2020) 003.
[43] M. Khodadi, A. Allahyari, S. Vagnozzi, and D. F. Mota, Black holes with scalar hair in light of the Event Horizon Telescope, J. Cosmol. Astropart. Phys. 09 (2020) 026.
[44] R. Konoplya, Shadow of a black hole surrounded by dark matter, Phys. Lett. B **795**, 1 (2019).
[45] V. I. Dokuchaev and N. O. Nazarova, Silhouettes of invisible black holes, Phys. Usp. **63**, 583 (2020).
[46] W. Javed, J. Abbas, and A. Övgün, Effect of the hair on deflection angle by asymptotically flat black holes in Einstein-Maxwell-Dilaton theory, Phys. Rev. D **100**, 044052 (2019).
[47] F. Long, J. Wang, S. Chen, and J. Jing, Shadow of a rotating squashed Kaluza-Klein black hole, J. High Energy Phys. 10 (2019) 269.
[48] R. Kumar and S. G. Ghosh, Black hole parameter estimation from its shadow, Astrophys. J. **892**, 78 (2020).
[49] D. Psaltis, Testing general relativity with the Event Horizon Telescope, Gen. Relativ. Gravit. **51**, 137 (2019).
[50] R. Konoplya, Quantum corrected black holes: Quasinormal modes, scattering, shadows, Phys. Lett. B **804**, 135363 (2020).
[51] K. Akiyama *et al.* (Event Horizon Telescope Collaboration), First M87 Event Horizon Telescope Results. I. The shadow of the supermassive black hole, Astrophys. J. **875**, L1 (2019).
[52] K. Akiyama *et al.* (Event Horizon Telescope Collaboration), First M87 Event Horizon Telescope Results. V. Physical origin of the asymmetric ring, Astrophys. J. Lett. **875**, L5 (2019).
[53] K. Akiyama *et al.* (Event Horizon Telescope Collaboration), First M87 Event Horizon Telescope Results. VI. The shadow and mass of the central black hole, Astrophys. J. Lett. **875**, L6 (2019).
[54] B. Abbott *et al.* (LIGO Scientific and Virgo Collaborations), Observation of Gravitational Waves from a Binary Black Hole Merger, Phys. Rev. Lett. **116**, 061102 (2016).
[55] E. P. Gross, Structure of a quantized vortex in boson systems, Nuovo Cimento (1955–1965) **20**, 454 (1961) [L. P. Pitaevskii, Sov. Phys. JETP **13**, 451 (1961)].
[56] R. Konoplya, A. Zhidenko, and A. Zinhailo, Higher order WKB formula for quasinormal modes and grey-body factors: Recipes for quick and accurate calculations, Classical Quantum Gravity **36**, 155002 (2019).
[57] H. Cho, A. Cornell, J. Doukas, and W. Naylor, Black hole quasinormal modes using the asymptotic iteration method, Classical Quantum Gravity **27**, 155004 (2010).
[58] S. Iyer and C. M. Will, Black hole normal modes: A WKB approach. 1. Foundations and application of a higher order WKB analysis of potential barrier scattering, Phys. Rev. D **35**, 3621 (1987).
[59] B. F. Schutz and C. M. Will, Black hole normal modes: A semianalytic approach, Astrophys. J. Lett. **291**, L33 (1985).
[60] R. Konoplya, Quasinormal behavior of the d-dimensional Schwarzschild black hole and higher order WKB approach, Phys. Rev. D **68**, 024018 (2003).
[61] S. Hawking, Particle creation by black holes, Commun. Math. Phys. **43**, 199 (1975).
[62] R. Konoplya and A. Zhidenko, Passage of radiation through wormholes of arbitrary shape, Phys. Rev. D **81**, 124036 (2010).
[63] S. H. Völkel, R. Konoplya, and K. D. Kokkotas, Inverse problem for Hawking radiation, Phys. Rev. D **99**, 104025 (2019).
[64] R. Konoplya, A. Zinhailo, and Z. Stuchlík, Quasinormal modes, scattering, and Hawking radiation in the vicinity of an Einstein-dilaton-Gauss-Bonnet black hole, Phys. Rev. D **99**, 124042 (2019).
[65] R. Konoplya and A. Zinhailo, Hawking radiation of non-Schwarzschild black holes in higher derivative gravity: A crucial role of grey-body factors, Phys. Rev. D **99**, 104060 (2019).
[66] V. Perlick, O. Y. Tsupko, and G. S. Bisnovatyi-Kogan, Influence of a plasma on the shadow of a spherically symmetric black hole, Phys. Rev. D **92**, 104031 (2015).
[67] C. Pekeris, Theory of propagation of sound in a half-space of variable sound velocity under conditions of formation of a shadow zone, J. Acoust. Soc. Am. **18**, 295 (1946).
[68] S. I. Badulin, V. I. Shrira, and L. S. Tsimring, The trapping and vertical focusing of internal waves in a pycnocline due to the horizontal inhomogeneities of density and currents, J. Fluid Mech. **158**, 199 (1985).
[69] S. I. Badulin and V. I. Shrira, On the irreversibility of internal-wave dynamics due to wave trapping by mean flow inhomogeneities. Part 1. Local analysis, J. Fluid Mech. **251**, 21 (1993).
[70] M. Mironov, Propagation of a flexural wave in a plate whose thickness decreases smoothly to zero in a finite interval, Sov. Phys. Acoust. **34**, 318 (1988).
[71] I. Z. Stefanov, S. S. Yazadjiev, and G. G. Gyulchev, Connection between Black-Hole Quasinormal Modes and Lensing in the Strong Deflection Limit, Phys. Rev. Lett. **104**, 251103 (2010).